Screening effects in the interplay between thermoelectric response and time-dependent driving

Nastaran Dashti,[1] Sara Kheradsoud,[2] Maciej Misiorny,[1] Peter Samuelsson,[2] and Janine Splettstoesser[1]

[1] *Department of Microtechnology and Nanoscience (MC2), Chalmers University of Technology, S-412 96 Göteborg, Sweden*
[2] *Department of Physics, Lund University, S-221 00 Lund, Sweden*

(Dated: September 6, 2019)

We investigate a coherent conductor, which is voltage- and temperature-biased and additionally fed by a time-dependently driven single-particle source (SPS). The conductor has an energy-dependent transmission that we propose to be realized by a quantum point contact (QPC). The interplay between stationary biases and time-dependent driving results in (quantum) screening effects at the QPC, which are already visible in the *linear* thermoelectric response coefficients of the conductor to small biases and which can literally be switched on and off by the presence or absence of the time-dependent driving. We find that this effect opens up for two very different opportunities for spectroscopy: (1) the linear-response coefficients modified by the source operation give direct access to rather unexplored quantum screening effects, which in other types of devices are obscured by geometric capacitive effects and only constitute negligibly small corrections. At the same time, (2) the tunable screening corrections to the linear-response coefficients are related to the energetic properties of the SPS, providing a direct experimental characterization tool for the SPS properties.

I. INTRODUCTION

This paper explores the combined transport properties of charge and heat in mesoscopic conductors. In recent years, there has been a growing interest in the field of nanoscale thermodelectrics [1]: by exploiting the properties of nanoscale conductors, such as their energy-dependent transmission properties, single-particle effects, and even quantum interference effects, novel principles for (electric) heat-to-work conversion are currently explored. In contrast to analogous macroscopic devices which are typically well characterized by their *linear* thermoelectric properties, the *nonlinear* response is of high interest for these nanoscale conductors, where applied temperature or voltage differences can easily be of the order of internal energy scales. However, the nonlinear operation of these devices goes along with complex quantum screening effects in the conductor, which impact its transmission properties [2–6]. Despite their relevance, these effects, in particular the effect of quantum (compared to geometrical) capacitances, have been little explored so far [7] and temperature-biased induced charges has to our knowledge not been experimentally accessed.

A very different reason for the study of charge and energy transport in mesoscopic conductors is the possibility to employ them as spectroscopy tools. Recently, spectroscopy of quantum transport has become relevant even on the *single-particle* level. The realization of different types of single-particle sources [8–10] for electronic conductors opens up perspectives for metrology, but also for electronic flying qubits and quantum optics experiments with single electrons. It is then highly relevant to not only explore the precision with which these particles are emitted [11–15], but also their detailed energetic properties [16, 17]. Various setups have been suggested to explore this, in particular also by studying combined charge and energy (or heat) transport [18–22]; but only few, rather complex experiments have until now been realized [23–26].

In this paper, we propose a setup, consisting of a thermally and electrically biased thermoelectric two-terminal conductor, additionally fed by a time-dependently driven (single-particle) source, and show that it can be exploited to address both urging questions introduced above. The proposed device, as shown in Fig. 1, is realized with a quantum point contact (QPC) with an energy-dependent transmission probability [27–30]. The single-particle

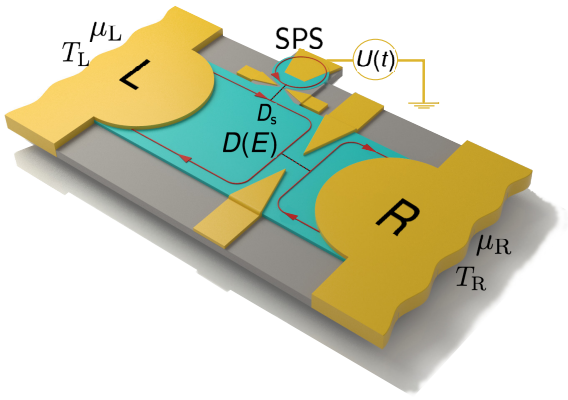

Figure 1. Schematic of a coherent mesoscopic conductor in the quantum Hall regime, connected to left and right reservoirs. A single-particle source (SPS), consisting of a slowly driven mesoscopic capacitor, injects electrons and holes into the conductor's edge state via a quantum point contact (QPC) with transparency D_s. Injected single particles are scattered by the central QPC with energy-dependent transparency $D(E)$ to electronic reservoirs L or R, with electrochemical potentials μ_L, μ_R and temperatures T_L, T_R.

source (SPS), which we employ here as an example is a time-dependently driven mesoscopic capacitor [31, 32], realized in a conductor in the quantum Hall regime [33]. Note however that our proposed schemes can equally be relevant for other types of time-dependently driven sources and other types of energy-dependent mesoscopic conductors. We find that the interplay between time-dependent driving and screening effects at the energy-dependent conductor due to the stationary biases, result in measurable and controllable corrections to the thermoelectric response, already in the *linear* response regime.

This has important consequences for transport spectroscopy: (i) the discovered corrections to the thermoelectric linear-response coefficients are directly proportional to different quantum screening coefficients, which usually only play a role in the nonlinear thermoelectric response of stationary conductors [2, 6, 34–38]. In the latter case they occur as higher-order correction effects, which are hard to extract from an experiment. In contrast, the correction terms identified here can be switched on and off by operating the additional time-dependent electron source. The quantum screening effects can thus directly be extracted by comparing standardly detected linear-response coefficients—in the presence and in the absence of an operating single-electron source. (ii) The discussed coefficients however also contain information about the SPS itself. Depending on which set of thermoelectric response coefficients is measured, tuning the potential landscape of the QPC allows to read out charge and heat currents injected from the SPS or even the full energy-resolved spectral currents.

In the following, we derive charge and heat currents flowing in the setup shown in Fig. 1, using a scattering matrix approach [39–42] and carefully considering geometrical and quantum screening effects of charge accumulation induced by both voltage and temperature biases. We then elaborate on concrete strategies how to exploit the interplay between screening effects and time-dependent driving in order to read out either until now elusive screening potentials or characteristic currents emitted from a SPS.

II. SETUP

We consider a coherent mesoscopic conductor, coupled to two electronic reservoirs L (left) and R (right), fed by a time-dependently driven SPS, see Fig. 1. In principle, any type of SPS is of interest here, such as voltage-bias induced Levitons [14, 15, 25, 43], dynamical quantum dots [24, 44–47], single-particle turnstiles [48, 49] or pumps [50–53]. However, in the present paper, we choose as an illustrative example a time-dependently driven mesoscopic capacitor [31, 32]. Such a setup was first realized as an electronic high-frequency SPS by Fève *et al.* [33] and has subsequently been implemented as crucial ingredient for quantum-optics-like experiments with single electrons [26, 54–56]. The mesoscopic capacitor, consisting of a small gate-confined region, is realized in the quantum Hall regime. It is weakly coupled to propagating quantum Hall edge states, indicated with red directional lines, by a QPC with (energy-independent) transmission probability D_s. As a result, the mesoscopic capacitor is characterized by a discrete energy-spectrum. A controlled driving of this energy spectrum by a time-periodic potential $U(t)$ results in a tunable emission of electron- and hole-like quasiparticles into the propagating edge state. Here, we assume this driving to be slow, such that single-particle excitations are emitted as minimal excitations of the Fermi sea in the conductor, see e.g. Ref. [57]. A detailed description of the mesoscopic capacitor in terms of its scattering matrix is given in Appendix A.

Electrons injected into the conductor from the SPS are sent onto a gate-tunable QPC with transparency[1] $D_0(E)$. The transmission probability of the QPC is *energy-dependent* and explicitly given by [27]

$$D_0(E) = \frac{1}{1+\exp\left[-\left(E-\epsilon\right)/\gamma\right]} \tag{1}$$

with the step energy (position) ϵ and smoothness γ. The energy dependence is used as critical property to break the electron-hole symmetry of the setup. As a result, particles emitted from the SPS are filtered depending on their energy. At the same time, the conductor shows a thermoelectric response, meaning that charge and heat currents non-trivially depend on the temperature and voltage biases, which can be applied between left and right contacts across the conductor. Here, we assume reservoir L to be grounded electrically, i.e. $\mu_L = \mu_0$, and kept at temperature $T_L = T_0$, while electrochemical potential and temperature in the reservoir R are assumed to be given by $\mu_R = \mu_0 - eV$ and $T_R = T_0 + \Delta T$, respectively. Here, $-e$ is the charge of the electron, with $e > 0$. In what follows, we set $\mu_0 \equiv 0$ as the reference energy.

III. THEORETICAL METHOD

In the following we are interested in the impact of currents injected by a time-dependently driven SPS on the linear thermoelectric response coefficients of the energy-dependent QPC. In order to theoretically investigate this impact, we employ a scattering matrix formalism, carefully taking care of screening effects arising at the QPC.

A. Charge and heat currents in scattering theory

We therefore start with a formulation of the full charge and energy currents in the presence of a time-dependent

[1] Note that this is the transmission probability in the absence of external biases.

driving and an arbitrarily energy-dependent QPC transmission. We choose reservoir R to be the one, where charge and heat currents are detected. The total time-averaged charge and energy currents in this reservoir can be described by time-dependent scattering theory [42] as

$$I_{\rm R} = I_{\rm s} + \frac{e}{h}\int dE\, D(E)\, \{f_{\rm R}(E) - f_{\rm L}(E)\}\,, \tag{2a}$$

$$I^E_{\rm R} = I^E_{\rm s} - \frac{1}{h}\int dE\, E\, D(E)\, \{f_{\rm R}(E) - f_{\rm L}(E)\}\,. \tag{2b}$$

Here, we have split the full currents into a contribution arising from the applied *stationary* temperature and voltage biases (second part of the right hand sides of Eq. (2)) and contributions, $I_{\rm s}$ and $I^E_{\rm s}$, arising from the time-dependently driven SPS in the presence of the energy-dependent transparency $D(E)$ of the QPC. Both current contributions depend on the transparency, which in turn depends on the applied electrical and thermal biases $D(E) = D(E, \{V, \Delta T\})$, due to screening effects, see the following Sec. III B. Note, that the transmission probability in Eq. (1) is the equilibrium one $D_0(E) = D(E, \{0, 0\})$. Furthermore, the Fermi functions $f_\alpha(E) = [1 + \exp([E - \mu_\alpha]/k_{\rm B}T_\alpha)]^{-1}$ enter the current expressions. The current contributions from the time-dependently driven SPS are given by the expressions

$$I_{\rm s} = \frac{e}{h}\sum_{n=-\infty}^{\infty} |S_n|^2 \int dE\, D(E)\, \{f_{\rm L}(E) - f_{\rm L}(E_n)\}\,, \tag{3a}$$

$$I^E_{\rm s} = -\frac{1}{h}\sum_{n=-\infty}^{\infty} |S_n|^2 \int dE D(E)\, E\, \{f_{\rm L}(E) - f_{\rm L}(E_n)\}\,. \tag{3b}$$

Here, S_n is the n-th Fourier component of the frozen scattering matrix of the slowly driven mesoscopic capacitor, see Appendix A for details. The index n in the energy-argument of the equilibrium Fermi functions, $f_{\rm L}(E) \equiv f_0(E) = [1 + \exp(E/k_{\rm B}T_0)]^{-1}$ corresponds to a shift of the energy by an integer multiple of the driving frequency of the capacitor, $E_n = E + n\hbar\Omega$.

In order to obtain the heat current from the current expressions given in Eq. (2), one needs to evaluate

$$J_{\rm R} = I^E_{\rm R} - V I_{\rm R}, \tag{4}$$

and analogous expressions for the separate components of the heat current arising from the stationary or time-dependently driven sources.

B. Screening effects

Away from equilibrium, due to an applied voltage or temperature bias, additional charge is injected into the QPC region. This charge is screened by charge redistributions at nearby metallic reservoirs and gates and by displacement currents flowing from the reservoirs, shifting the electrostatic potential at the QPC and hence its scattering properties [2, 6, 37, 38]. To account for the voltage and temperature dependence of the transmission probability, we thus need to characterize the electrostatic environment of the QPC as well as how the scattering properties depend on the electrostatic potential. Here we follow Refs. [37, 38] and consider a model of the QPC with two constant potential regions, one on each side of the QPC. The size of these regions, where the charge is not perfectly screened, is given by the screening length λ. We calculate the scattering properties of the QPC within a semi-classical, WKB approach; a detailed description of the general model is given in Appendix B. Here, we consider a spatially symmetric setup, capturing all the relevant physics. In the setup, the constant potential regions are equally capacitively coupled to both the QPC split-gate electrodes, with capacitance $C_{\rm g}$, and to respective electronic reservoir, with capacitance C. The capacitive coupling between the two constant potential regions does not affect the result in the symmetric case. All other capacitive couplings are assumed to have a negligibly small influence on the screening properties. We note that, in principle, screening at the QPC of the electrons and holes injected from the SES also should be accounted for. Here we however neglect this dynamical, ac-screening effect, since we expect this to be mostly of importance in time-resolved transport quantities, which are not considered in the present paper.

The details of the calculation of the voltage and temperature dependence of the transmission probability, closely following Ref. [38], are deferred to Appendix B. Focusing on the weakly non-linear regime, properly accounting for gauge-invariance, and expanding to first order in $V, \Delta T$, we have

$$D(E, \{V, \Delta T\}) = D_0(E) - \frac{dD_0}{dE}\left(\xi eV + \chi k_{\rm B}\Delta T\right). \tag{5}$$

Here, we define the dimensionless coefficients

$$\xi = \frac{2C + \mathcal{D}}{2C + \mathcal{D} + 2C_{\rm g}}, \quad \chi = \frac{\mathcal{D}^E}{2C + \mathcal{D} + 2C_{\rm g}} \tag{6}$$

with $\mathcal{D} = -e^2\int dE\nu(E)df/dE$ and $\mathcal{D}^E = -e^2\int dE[E/(k_{\rm B}T_0)]\nu(E)df/dE$, where $\nu(E)$ is the total density of states in the two constant potential regions. The density of states is calculated semi-classically for an effectively one-dimensional QPC scattering potential, described by an inverted parabola $U(x) = \epsilon - m\omega^2x^2/2$, where m is the effective electron mass and ω determines the smoothness of the barrier as $\gamma = 2\hbar\omega$. It is given by [37] $\nu(E) = (\gamma\pi)^{-1}\mathrm{arcosh}\left(\sqrt{E_\lambda/(\epsilon - E)}\right)$ for energies $\epsilon - E_\lambda < E < \epsilon$ and $\nu(E) = (\gamma\pi)^{-1}\mathrm{arsinh}\left(\sqrt{E_\lambda/(E - \epsilon)}\right)$ for energies $E > \epsilon$, with $E_\lambda = m\omega^2\lambda^2/2$ the energy scale related to the screening length λ.

The coefficients ξ and χ depend on the capacitances $C, C_{\rm g}$, the background temperature T_0 and also on the

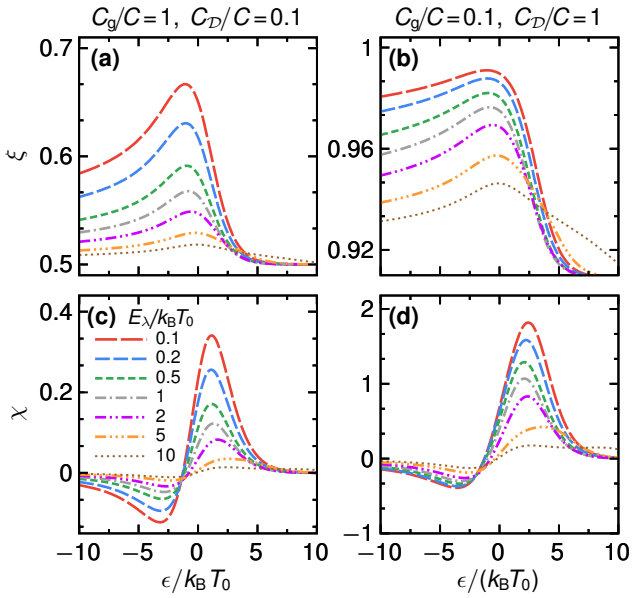

Figure 2. Coefficients ξ, in (a), (b), and χ, in (c),(d) as a function of $\epsilon/(k_BT_0)$ for a set of different $E_\lambda/(k_BT_0)$, see legend in (c), and for different values of the parameters C_g/C and $C_{\mathcal{D}}/C$.

energy scales of the scatterer $\epsilon, \gamma, E_\lambda$ via $\mathcal{D}$ and $\mathcal{D}^E$. A detailed analysis, see Appendix B, shows that ξ, χ can conveniently be expressed in terms of four dimensionless parameters $C_g/C, C_{\mathcal{D}}/C, \epsilon/(k_BT_0)$ and $E_\lambda/(k_BT_0)$, where $C_{\mathcal{D}} = e^2E_\lambda/(8\pi\gamma k_BT_0)$ gives the typical magnitude of $\mathcal{D}, \mathcal{D}^E$. The coefficient $0 \le \xi \le 1$ is bounded from above by gauge invariance, while χ can have any sign and is not bounded. From Eq. (6) it follows that in the limit of dominating capacitive coupling to the gate, $C_g \gg C, C_{\mathcal{D}}$ both coefficients are small, $\xi, \chi \ll 1$. However, there are also extended parameter regimes, where ξ and χ are considerably large, as can be seen in Fig. 2, where we plot both coefficients as a function of ϵ for a representative set of parameters.

We see that ξ shows a qualitatively similar behavior in both panels, Figs. 2 (a) and (b), with a maximum around $\epsilon/(k_BT_0) = 0$, approaching $C/(C + C_g)$ for $\epsilon/(k_BT_0) \to \infty$ and decaying slowly with increasingly negative $\epsilon/(k_BT_0) < 0$. The magnitude of the variations with ϵ is however larger for $C_g \gg C_{\mathcal{D}}$. The trend is the opposite for χ, in panels Figs. 2 (c) and (d), with larger magnitude of ϵ variations for $C_{\mathcal{D}} \gg C_g$. Overall, χ shows a qualitatively similar, alternating-sign behavior in both panels, with a negative peak at $\epsilon < 0$ and a positive peak at $\epsilon > 0$, both of the order of k_BT_0 away from the origin. For larger absolute values χ approach zero for $\epsilon/(k_BT_0) \to \pm\infty$.

IV. OPPORTUNITIES FOR SPECTROSCOPY

A. Linear thermoelectric response

Starting from the general expressions for the charge and energy currents, Eqs. (2a) and (2b), and the expression for the transmission probability in Eq. (5), we can derive expressions for I_R and J_R to leading order in the applied biases, ΔT and V. It is convenient to write the currents in a vector form as

$$\begin{pmatrix} I_R \\ J_R \end{pmatrix} = \begin{pmatrix} I_s^{\rm dir} \\ I_s^{E,\rm dir} \end{pmatrix} + \begin{pmatrix} G+G_s & L+L_s \\ M+M_s & K+K_s \end{pmatrix} \begin{pmatrix} V \\ \Delta T \end{pmatrix}. \tag{7}$$

Discussing the different terms one by one, we first have the "direct" source currents modified by the energy-dependent transmission, which to leading order is not affected by the applied biases, that is, $I_s^{\rm dir} = I_s|_{\Delta T, V=0}$ and $I_s^{E,\rm dir} = I_s^E|_{\Delta T, V=0}$, with I_s, I_s^E given in Eqs. (3a) and (3b). Second, the matrix elements G, L, M and K are the standard, linear response, thermoelectric coefficients

$$G = \frac{e^2}{h}\mathcal{I}_0, \quad L = -\frac{M}{T_0} = \frac{e}{h}k_B\mathcal{I}_1, \quad K = -\frac{1}{h}(k_B^2T_0)\mathcal{I}_2, \tag{8}$$

(see, e.g,. Ref. [1] for a review) with

$$\mathcal{I}_n = \int_{-\infty}^{\infty} dE\, D_0(E)\left(\frac{E}{k_BT_0}\right)^n\left(-\frac{\partial f_0(E)}{\partial E}\right). \tag{9}$$

Here, G is the electrical conductance, K the thermal conductance, and L, M thermoelectric coefficients related to the Seebeck and Peltier coefficients. We emphasize that none of these coefficients are affected by the screening effects. Third, of main interest here, are the coefficients G_s, L_s, M_s and K_s, modifying the standard linear response result. Physically, the origin of these coefficients is that the applied biases lead to a potential- and temperature-dependent transmission probability, $D(E)$, which in turn modifies the currents emitted from the SPS, when they are scattered at the QPC. Put differently, the coefficients all arise due to the interplay between the non-equilibrium induced screening effects and the time-periodically driven source currents. The expressions for the coefficients are

$$\begin{aligned} G_s &= \xi\frac{e^2}{h}\mathcal{J}_0, & L_s &= \chi\frac{k_Be}{h}\mathcal{J}_0, \\ M_s &= -\xi\frac{k_Be}{h}T_0\mathcal{J}_1, & K_s &= -\chi\frac{k_B^2T_0}{h}\mathcal{J}_1, \end{aligned} \tag{10}$$

where

$$\mathcal{J}_n = \sum_n |S_n|^2 \int dE \frac{dD_0(E)}{dE}\left(\frac{E}{k_BT_0}\right)^n [f_0(E) - f_0(E_n)]. \tag{11}$$

Interestingly, the charge-current and heat-current coefficients are related in a simple way

$$\frac{G_s}{e\xi} = \frac{L_s}{k_B\chi}, \quad \frac{M_s}{e\xi} = \frac{K_s}{k_B\chi} \tag{12}$$

which derives from the fact that the two pairs of coefficients, $G_\mathrm{s}, M_\mathrm{s}$ and $L_\mathrm{s}, K_\mathrm{s}$, respectively stem from potential- and temperature-induced screening effects. The relation, Eq. (12), demonstrates that the total coefficient matrix in Eq. (7) does not satisfy Onsager's symmetry relations. We stress that this breakdown is to be expected, due to the external driving breaking time-reversal symmetry. Namely, the treatment of this external driving is not limited to linear response.

1. *Weak thermoelectric effect*

The origin of the coefficients in Eq. (10) as an interplay between the screening effects and the source currents becomes explicit in the limit of a weak thermoelectric effect, that is, for a QPC constituting a smoothly energy-dependent barrier. In this limit we can expand the transmission probability to first order in energy as $D_0(E) \approx D_0 + ED_0'$, where $D_0 \equiv D_0(0)$ and $D_0' \equiv dD_0(E)/dE|_{E=0}$. Inserting this expansion into the coefficient expressions given in Eq. (10) we arrive at the relations

$$G_\mathrm{s} = \frac{h}{e^2}\frac{1}{\mathcal{L}_0 T_0}\xi L I^\mathrm{dir}_{\mathrm{s},0}, \qquad M_\mathrm{s} = \frac{h}{e^2}\frac{1}{\mathcal{L}_0 T_0}\xi L J^\mathrm{dir}_{\mathrm{s},0} \tag{13}$$

with the Lorenz number $\mathcal{L}_0 = \frac{\pi^2 k_\mathrm{B}^2}{3e^2}$. Equivalent relations for L_s and K_s are directly obtained from these expressions, when employing Eq. (12). Here, $I^\mathrm{dir}_{\mathrm{s},0}$ and $J^\mathrm{dir}_{\mathrm{s},0}$ are the charge and heat currents that would flow into reservoir R for a completely open QPC, $D(E) \to 1$, and in the absence of biases. The thermoelectric coefficient is given by $L = \frac{e\pi^2}{3h}k_\mathrm{B}^2 T_0 D_0'$, in accordance with Mott's law. Importantly, the conductance correction to all Onsager coefficients, G_s, L_s, M_s, and K_s become particularly simple in this regime. They are proportional to the bare charge or heat source currents, $I^\mathrm{dir}_{\mathrm{s},0}$ or $J^\mathrm{dir}_{\mathrm{s},0}$, to the screening coefficients ξ and χ, and to the same unperturbed thermoelectric coefficient L.

B. Sensing of (quantum) screening effects using time-dependent current emitters

In typical, purely stationary biased conductors, the screening effects, introduced in Sec. IV A above, occur as higher-order corrections to the standard linear-response coefficients, when the voltage and temperature biases are of the order of or larger than relevant internal energy scales of the conductor. To clearly distinguish—possibly negligibly small—higher-order correction terms from the dominating linear, first-order response is however difficult in realistic experiments. Furthermore, screening effects due to temperature have not been observed so far. In the present manuscript, we reveal an interplay effect between time-dependent source driving and (quantum) screening effects, which allows to directly read out the latter from the modifications of the linear-response coefficients due to the driving, G_s, L_s, M_s, and K_s. Note that these are not simply uncontrolled small corrections to the standard, stationary linear-response coefficients, but can be switched on and off by the source at will. In other words, the difference between the full linear response of the device in the absence and presence of the driven source directly yields the sought-for modified terms.

For the specific readout, we can distinguish two situations: (i) the weak thermoelectric case, where at the same time the source properties are well known, and (2) the general case of arbitrary $D(E)$ where we neither assume a detailed knowledge of the source properties.

In case (i), Eqs. (13) and (12) determine the modifications of the linear-response coefficients. One can determine $I^\mathrm{dir}_{\mathrm{s},0}$ (respectively $J^\mathrm{dir}_{\mathrm{s},0}$) and L from separate electrical (or thermal) dc-current measurements, where only the source is active or the thermal bias is applied. Thus, we can subsequently directly extract the coefficients ξ and χ, given in Eq. (6). Note that these parameters can already be obtained from a measurement of the charge-current coefficients G_s and L_s, alone. If further measurements of M_s and K_s are possible, they would provide an independent possibility to verify the obtained parameters.

In case (ii), the functions $\mathcal{J}_0$ and $\mathcal{J}_1$ are not necessarily known. An experiment could then have two strategies to proceed: either a measurement of all four coefficients, G_s, L_s, M_s, and K_s, gives access to the four unknown functions χ, ξ, $\mathcal{J}_0$ and $\mathcal{J}_1$, allowing to determine χ and ξ, separately. Or, in an experiment, e.g. restricted to a measurement of charge-current coefficients only, one could extract the ratio

$$\frac{\chi}{\xi} = \frac{e}{k_\mathrm{B}}\frac{L_\mathrm{s}}{G_\mathrm{s}} = \frac{\mathcal{D}^E}{2C + \mathcal{D}}. \tag{14}$$

Note that this ratio gives access to, until now undetected, quantum screening properties due to a thermal bias, encoded in $\mathcal{D}^E$.

C. Characterization of single-electron sources with energy-selective transport spectroscopy

Importantly, the fact that the time-dependently driven SPS impacts the linear response coefficients, allows for identifying direct relations between the modified response coefficients, G_s, L_s, M_s, and K_s, and the signal injected from the SPS. More specifically, in this section, we demonstrate, how the thermoelectric response of the conductor shown in Fig. 1 can be used for a readout of the spectral current of the source as well as of the bare source charge and heat currents.

1. *Sharp QPC transmission*

We start by approximating the transmission of the QPC by a sharp step. This approximation matches the

experimental situation when the temperature T_0 is small with respect to the broadening γ of the transmission given in Eq. (1). We thus here assume

$$D(E) \approx \theta(E-\epsilon) \tag{15}$$

Note that insightful, analytical results for the full current expressions, using this sharp-step approximation can be found; they are explicitly shown in Appendix C. In this regime, it is reasonable to further assume that the geometric capacitances are the only relevant ones. This also means that there is no dependence on the QPC step height or smoothness in the screening-induced prefactors, χ and ξ, of the coefficient corrections. Furthermore, taking the geometric capacitances to be symmetric to the left and right side of the QPC and smaller than the capacitive coupling to the gate controlling the QPC, we have $\xi = \frac{1}{2}$. A generalization of these assumptions is straightforward and will be treated elsewhere.

Using Eqs. (10) and (11), we then find the modification of the charge conductance, G_s, to be given by

$$\frac{G_\mathrm{s}}{e^2/2h} = i(\epsilon) \tag{16}$$

where $i(\epsilon)$ is the spectral current of the source (the energetic distribution of particles) at the step height energy of the QPC, ϵ. The spectral current is determined by

$$i(E) = \sum_{n=-\infty}^{\infty} |S_n|^2 \left[f_\mathrm{L}(E_n) - f_\mathrm{R}(E)\right] \ . \tag{17}$$

As a result, measuring the difference of the charge conductance of the system in the absence and presence of the time-dependently driven SPS, gives direct access to the spectral current of the emitted particles. By tuning the step height of the QPC transmission, the full spectral current can be read out. The result is shown in Fig. 3 (a) for different temperatures T_0. A detailed discussion of the temperature dependence of this spectral current has been discussed in Ref. [57], where it has been found to be a characteristic feature of the type of employed SPS. Note that a similar procedure has been employed in Ref. [23], where the response of the source-injected charge current to a modulation of the gate potential, defining the energy-selective barrier, was used to read out the spectral current emitted far above the Fermi sea by a dynamically modulated quantum dot. Here, we show that the response to externally applied biases gives similar opportunities, but opens up for a broader set of characteristic response coefficients.

Indeed, also the modification of the thermoelectric coefficient M_s contains information on the spectral current, but also contains the full direct charge current from the source. We find

$$M_\mathrm{s} = -\frac{e}{2h}\ \epsilon\ i(\epsilon) + I_\mathrm{s}^\mathrm{dir}. \tag{18}$$

In Fig. 3 (b), we show M_s as function of the step height for different background temperatures. Reading out M_s hence allows for the readout of $I_\mathrm{s}^\mathrm{dir}$ after a measurement of G_s has lead to the extraction of the spectral current. Alternatively, an independent measurement of the spectral current is provided by M_s in case the average source charge current, $I_\mathrm{s}^\mathrm{dir}$, is known.

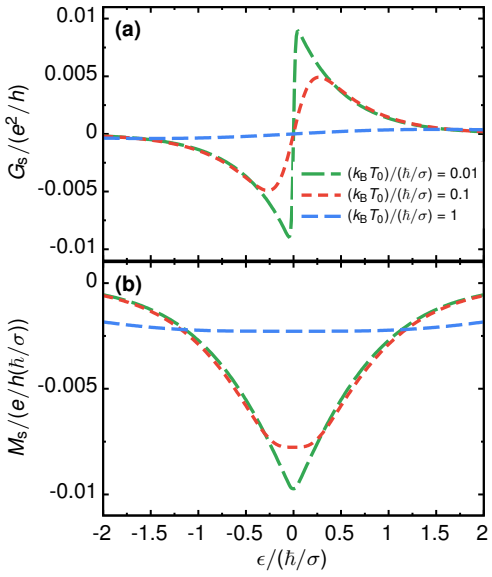

Figure 3. Modification of (a) the charge conductance G_s and (b) the thermoelectric coefficient M_s, as function of the step height $\epsilon/(\hbar/\sigma)$ in the QPC transmission and for different values of the background temperature T_0. Here, σ is the width in time of the current pulses injected from the SPS.

Importantly, in general the modifications of the thermal conductance, K_s, and the thermoelectric coefficient L_s contain the same source information as G_s and M_s and only differ by a factor given by the potential- and temperature-bias induced screening properties of the QPC and the background temperature, see Eq. (12). An additional measurement of the modification of the linear-response coefficients due to temperature-induced screening can therefore be used for an independent control of the observables extracted from a measurement of G_s and M_s.

2. *Smooth QPC transmission*

We now discuss the opposite case of a very weakly energy-dependent QPC. This is of relevance when the background temperature is small, $k_\mathrm{B}T_0 \ll \gamma$ and transport (both due to the small biases as well as due to the driven source) take place in an energy window, which is inferior to the broadening of the step-like QPC transmission. In this regime of *weak* thermoelectricity, as presented in Sec. IV A 1, the energy dependence of the QPC transmission is large enough to make the interplay between screening effects and time-dependent driving visible, without however strongly modifying the contributions from the different inputs, see Eqs. (13).

As a result, the modifications of the linear thermoelectric response coefficients, G_s, L_s, M_s, and K_s are directly proportional to the *unperturbed* charge- and heat currents, $I^\mathrm{dir}_{\mathrm{s},0}$ and $J^\mathrm{dir}_{\mathrm{s},0}$, injected from the SPS. A measurement of the linear response coefficients in the absence and presence of the driven SPS therefore allows to read out these charge- and heat currents, which the source would emit without external stationary biases, V and ΔT, and without a beam-splitting QPC.

The four coefficients given in Eqs. (13) contain the easily accessible background temperature T_0 and stationary thermoelectric response coefficient L. These two quantities can hence be assumed as known parameters. This means that the four coefficients contain maximally four unknown quantities: the screening coefficients χ and ξ and the sought-for source currents $I^\mathrm{dir}_{\mathrm{s},0}$ and $J^\mathrm{dir}_{\mathrm{s},0}$.

Note however that even if the experiment is limited to the extraction of a subset of these coefficients, valuable information about the source currents is still accessible. For example, in an experiment where quantum screening is absent and hence no screening occurs due to a temperature bias, the ratio between $I^\mathrm{dir}_{\mathrm{s},0}$ and $J^\mathrm{dir}_{\mathrm{s},0}$ is still accessible from a measurement of G_s and M_s. Knowledge of the (geometrical) screening factor ξ would even allow to extract both charge- and heat currents separately. Furthermore, if in an experiment only the modifications to the charge current coefficients, G_s and L_s, can be detected, while heat currents are not detectable, the source charge current could still be read out, to a degree that depends on the knowledge of the screening factors.

V. CONCLUSIONS

In summary, we have shown how the interplay between time-dependent driving and quantum screening effects due to stationary thermal and electrical biases impacts the linear response of a thermoelectric conductor. This allows us to put forward two very different proposals for transport spectroscopy. The first proposal suggests how to directly read out, until now elusive quantum screening effects, from tunable modifications of linear-response coefficients due to the time-dependent driving of a side-coupled (single-particle) source. Importantly the concrete properties of the SPS do not necessarily have to be precisely known to allow for this readout. We expect presently available experimental techniques to allow for the proposed readout of quantum screening effects. The findings of such an experiment could be used to test predictions for screening potentials, as given in detail in Appendix B.

At the same time, we suggest that these controllable contributions to the thermoelectric response coefficients can also be employed in order to read out charge and heat currents and even energy-resolved currents injected from the SPS. A full readout of these observables can be performed by carefully tuning the potential defining the QPC, which is a central element of the proposed setup. We thereby extend a technique employed in Refs. [23, 24], where the charge current response to the gate-voltage tuning of an energy-selective conductor has been used for the readout of spectral currents injected from a dynamical quantum dot. Here, we show that also the response to external biases allows for such a readout and thereby provides a full set of response coefficients which can independently provide information on the spectral current and other transport observables.

ACKNOWLEDGMENTS

Funding from the Knut and Alice Wallenberg Foundation through the Academy Fellow program (J.S., N.D. and M.M.), and from the Swedish VR is gratefully acknowledged.

Appendix A: Time-dependently driven mesoscopic capacitor

In this appendix, we briefly summarize how to describe the time-dependently mesoscopic capacitor with a Floquet scattering method [42] in the regime of our interest. This explicit calculation is relevant only for plots of the extracted spectral currents via thermoelectric response coefficients as presented in Sec. IV C. There, we are interested in an ideal source that emits well-separated pulses, see e.g. Ref. [57] for a detailed discussion.

The mesoscopic capacitor has a discrete level spectrum with level spacing Δ and level width Γ. The level width is $\Gamma = D_\mathrm{s}\Delta/(4\pi)$; it hence depends on the coupling between the mesoscopic capacitor and the propagating edge states, see Fig. 1. To allow for the emission of well-separated pulses, the level width should be much smaller than the level spacing, $\Gamma \ll \Delta$, requiring $D_\mathrm{s} \ll 1$. We further assume that only one level of the mesoscopic capacitor contributes to the emission process. If finally the driving is slow and the driving amplitudes are conveniently chosen, the time interval between the electron emission t^e (namely the time at which the level of the mesoscopic capacitor crosses the Fermi level, from below) and the hole emission t^h is long enough so that a particle is definitely emitted before the next level crossing. This translates as

$$|t^e - t^h| \gg \sigma, \tag{A1}$$

where 2σ is the width of the pulse in time. In particular this also means $\Omega\sigma \ll 1$.

In this regime, the scattering matrix gets the form

$$S_n(E) = \begin{cases} -2\Omega\sigma \mathrm{e}^{-n\Omega\sigma}\mathrm{e}^{in\Omega t^e}, & n > 0, \\ -2\Omega\sigma \mathrm{e}^{n\Omega\sigma}\mathrm{e}^{in\Omega t^h}, & n < 0, \\ 1, & n = 0. \end{cases} \tag{A2}$$

Note that $S_n(E)$ has to be unitary and needs to fullfill $\sum_n |S_n(E)|^2 = 1$.

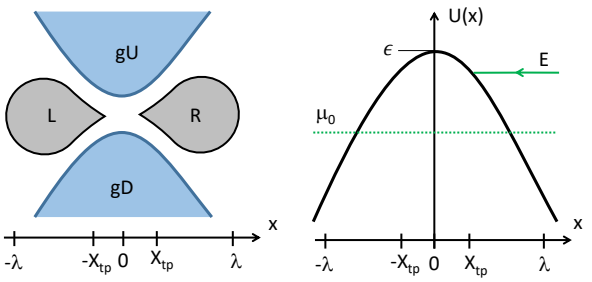

Figure 4. (a) Schematic top-view of QPC, showing regions L and R where the charge is not screened. The upper (gU) and lower (gD) split gate electrodes are also shown. (b) Energy and potential sketch. At the QPC, the electrostatic potential can be approximated by an inverted parabola, with top energy ϵ. The width of the potential parabola determines the smoothness γ of the barrier. For further details see text.

Appendix B: Screening effects in weakly nonlinear response

In this section we provide a detailed discussion of the effect of screening in the weakly non-linear transport regime. Various aspects of the result have been presented in different papers over several decades, see e.g. Refs. [2, 6, 34–38]. However, it is our impression that a complete, self-consistent discussion is missing. Since the material is mainly known but still is of central interest to our work, we present it in detail in this appendix.

1. QPC potential, screening regions and semi-classical approach

In Fig. 4, left panel, we show a schematic top-view of the QPC region sketched in Fig. 1. We assume that there is only one conduction mode open in the QPC and that the problem hence is effectively 1D, along the x-axis. Indicated in the figure are two regions, L and R, on each side of the QPC midpoint at $x = 0$. In these two regions, of the size of the screening length λ, it is assumed that the charge is not completely screened. The electrostatic potential $U(x)$ of the QPC is taken to be an inverted parabola [27, 58], see right panel of Fig. 4, with

$$U(x) = \epsilon - \frac{m\omega^2}{2}x^2 \ , \tag{B1}$$

where ϵ determines the top of the potential, at $x = 0$. Here, m is the effective mass of the electron and $\hbar\omega/2 = \gamma$, where γ is the smoothness of the transmission probability.

Let's now consider an electron incident from e.g. the right at an energy E, where the energy is counted from $\mu_0 \equiv 0$, the electrochemical potential of the reservoirs at equilibrium. This is shown in panel (b) of Fig. 4. Using a semiclassical, WKB analysis, the electron has a classical turning point at a position $x_{\rm tp} = x_{\rm tp}(E)$, obtained from $E = \epsilon - m\omega^2 x_{\rm tp}^2/2$, that is

$$x_{\rm tp} = \sqrt{\frac{2(\epsilon - E)}{m\omega^2}}. \tag{B2}$$

As a consequence we can say that the regions 1 and 2, where charges are not fully screened, are defined by

$$-\lambda < x < -x_{\rm tp}, \quad x_{\rm tp} < x < \lambda \tag{B3}$$

respectively, as shown in Fig. 4 (a). We note that the expression for $x_{\rm tp}$ formally holds only for $E < \epsilon$. For $E > \epsilon$, the result would be non-physical (imaginary) and we instead take $x_{\rm tp} = 0$, that is, there is no classical turning point and region 1 and 2 are in direct contact. Moreover, for sufficiently low energies $E_{\rm min}$, the turning point $x_{\rm tp}(E)$ reaches the boundaries of the non-perfectly screened region. This happens when $x_{\rm tp} = \lambda$, which gives $E_{\rm min} = \epsilon - E_\lambda$, where we introduced for later convenience $E_\lambda = m\omega^2\lambda^2/2$.

2. Scattering matrix, semiclassical approach

To find the scattering matrix S for the QPC, we point out that the length of the scattering region is taken to be $-\lambda < x < \lambda$. We first note that, quite generally, the scattering matrix for the QPC can be written as

$$S = \begin{pmatrix} ie^{i\phi(E)}\sqrt{1-D(E)} & e^{i\phi(E)}\sqrt{D(E)} \\ e^{i\phi(E)}\sqrt{D(E)} & ie^{i\phi(E)}\sqrt{1-D(E)} \end{pmatrix} \ , \tag{B4}$$

where we take into account that the QPC is spatially symmetric and impose the unitarity condition for S, i.e. $S^\dagger S = 1$. The transmission probability $D(E)$ is given by Eq. (1) in the main text,

$$D(E) = \frac{1}{1 + e^{-(E-\epsilon)/\gamma}}. \tag{B5}$$

The scattering phase $\phi(E)$ is the dynamical phase acquired when traversing the QPC. Starting with the case $E_{\rm min} < E < \epsilon$, it is obtained by integrating the semiclassical, position-dependent momentum $p(x) = \sqrt{2m[E - U(x)]}$ over the path through region L and R,

$$\phi(E) = \frac{\sqrt{2m}}{\hbar}\left(\int_{-\lambda}^{-x_{\rm tp}} dx + \int_{x_{\rm tp}}^{\lambda} dx\right)\sqrt{E - \epsilon + \frac{m\omega^2}{2}x^2} \tag{B6}$$

giving

$$\begin{aligned}\phi(E) &= \frac{m\omega x_{\rm tp}^2}{\hbar}\times \\ &\left[\frac{\lambda}{x_{\rm tp}}\sqrt{\left(\frac{\lambda}{x_{\rm tp}}\right)^2 - 1} - \ln\left(\frac{\lambda}{x_{\rm tp}} + \sqrt{\left(\frac{\lambda}{x_{\rm tp}}\right)^2 - 1}\right)\right] \\ &= \frac{\epsilon - E}{\gamma}\times \\ &\left[\sqrt{\frac{E_\lambda}{\epsilon - E}\left(\frac{E_\lambda}{\epsilon - E} - 1\right)} - \operatorname{arcosh}\left(\sqrt{\frac{E_\lambda}{\epsilon - E}}\right)\right] \ ,\end{aligned} \tag{B7}$$

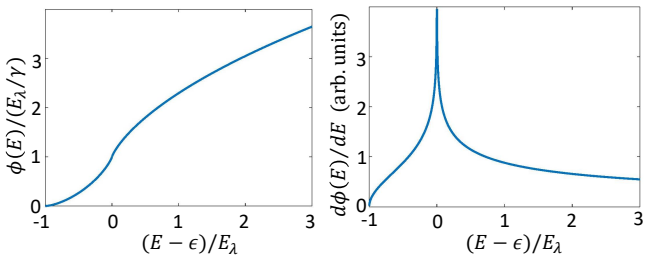

Figure 5. (a) Normalized scattering phase as a function of energy. (b) Energy derivative of the scattering phase, proportional to the density of states (see text).

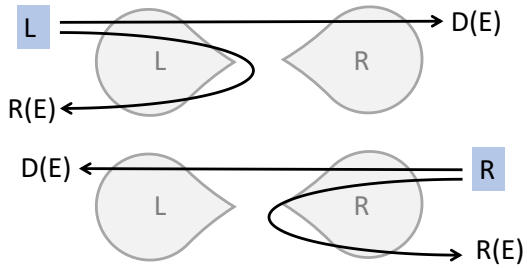

Figure 6. Schematic of scattering paths contribution to the density of states.

where we used that the prefactor $m\omega x_{\rm tp}^2/\hbar = (\epsilon - E)/\gamma$.

For energies $E < E_{\rm min}$ the acquired phase is zero. For energies above the potential top, $E > \epsilon$, $x_{\rm tp} = 0$ and we can proceed as above and write the acquired phase

$$\phi(E) = \frac{1}{\hbar}\int_{-\lambda}^{\lambda} dx \sqrt{2m\left(E - \epsilon + \frac{m\omega^2}{2}x^2\right)} \tag{B8}$$

giving

$$\phi(E) = \frac{E-\epsilon}{\gamma}\times \left[\sqrt{\frac{E_\lambda}{E-\epsilon}\left(\frac{E_\lambda}{E-\epsilon}+1\right)} + \text{arsinh}\left(\sqrt{\frac{E_\lambda}{E-\epsilon}}\right)\right] . \tag{B9}$$

We note that the phase, in addition to the amplitudes, depends on the energy scale E_λ. In Fig. 5, the normalized phase $\phi(E)/(E_\lambda/\gamma)$, is plotted as a function of energy $(E-\epsilon)/E_\lambda$. It is clear that the phase has a cusp at $E = \epsilon$.

We stress that it is in principle possible to perform a full quantum mechanical calculation of the scattering matrix elements, following Refs. [58, 59]. Since the main interest here is to get a qualitative picture of the physics, we however judge that a semiclassical treatment is sufficient.

3. Density of states and injectivities

The next step is to consider the density of states (DOS). It is known [60, 61] that the global DOS, $\nu(E)$, of an arbitrary scatterer is related to the scattering matrix S as

$$\nu(E) = \frac{1}{2\pi i}\text{tr}\left[S^\dagger \frac{dS}{dE}\right] = \frac{1}{\pi}\frac{d\phi(E)}{dE} . \tag{B10}$$

From the expressions for $\phi(E)$ above, we have, for $E_{\rm min} < E < \epsilon$,

$$\nu(E) = \frac{1}{\gamma\pi}\text{arcosh}\left(\sqrt{\frac{E_\lambda}{\epsilon - E}}\right) \tag{B11}$$

and for $E > \epsilon$ we have

$$\nu(E) = \frac{1}{\gamma\pi}\text{arsinh}\left(\sqrt{\frac{E_\lambda}{E-\epsilon}}\right) \tag{B12}$$

in line with Ref. [37], see also Sec. III B. In Fig. 5, we plot the energy derivative of the phase. It is clear that the phase derivative has a singularity at $E = \epsilon$, a consequence of the semiclassical approximation. As is clear below, this singularity is integrable, that is, it does not prevent an analysis of the energy integrated DOS, entering the final result.

We note that since the QPC is symmetric, half of the states are on each side of the saddle point, such that

$$\nu_{\rm L}(E) = \nu_{\rm R}(E) = \nu(E)/2 . \tag{B13}$$

Here $\nu_\alpha(E)$ is thus the local density of states in the regions $\alpha =$ L,R, see Fig. 4. Based on the local density of states, we can follow the discussion in Ref. [36] to calculate the partial density of states and the related injectivities for the QPC. To this aim, it is helpful to consider the trajectories for incoming particles from the left and right, shown in Fig. 6. From these paths we can write down the local, partial density of states $\nu_{\alpha\beta\gamma}$, where $\gamma =$ L,R denotes the reservoir from which a particle is incident on the scatterer, $\alpha =$ L,R denotes the reservoir to which the particle is emitted from the scatterer, and $\beta =$ L,R denotes the region of the density of states to which the path contributes. This gives, by inspection, writing out all eight cases explicitly,

$$\begin{aligned}
\nu_{\rm LLR}(E) &= \frac{1}{2}D(E)\nu_{\rm L}(E), \quad \nu_{\rm LLL}(E) = R(E)\nu_{\rm L}(E),\\
\nu_{\rm RLL}(E) &= \frac{1}{2}D(E)\nu_{\rm L}(E), \quad \nu_{\rm RLR}(E) = 0,\\
\nu_{\rm LRR}(E) &= \frac{1}{2}D(E)\nu_{\rm R}(E), \quad \nu_{\rm LRL}(E) = 0,\\
\nu_{\rm RRL}(E) &= \frac{1}{2}D(E)\nu_{\rm R}(E), \quad \nu_{\rm RRR}(E) = R(E)\nu_{\rm R}(E),
\end{aligned} \tag{B14}$$

Here $D(E)$ and $R(E) = 1 - D(E)$ are the probabilities for the different paths to occur, given that one particle is incident from the reservoir. The factor 1/2 in front of

the terms with $D(E)$ tells that the particle only traverses the region in one direction (out of two possible), thus contributing to only one half of the total DOS. We stress that the following relation holds

$$\sum_{\alpha,\beta,\gamma} \nu_{\alpha\beta\gamma}(E) = \nu_{\rm L}(E) + \nu_{\rm R}(E) = \nu(E). \quad \text{(B15)}$$

From the partial, local DOS we can construct the injectivities $\nu_{\beta\gamma}(E)$ by summing over the reservoirs to which the particle is emitted. Explicitly, we have

$$\begin{aligned}
\nu_{\rm LL}(E) &= \nu_{\rm LLL}(E) + \nu_{\rm RLL}(E) = \frac{1}{2}D(E)\nu_{\rm L}(E) \\
\nu_{\rm RR}(E) &= \nu_{\rm LRR}(E) + \nu_{\rm LRR}(E) = \frac{1}{2}D(E)\nu_{\rm R}(E) \\
\nu_{\rm RL}(E) &= \nu_{\rm LRL}(E) + \nu_{\rm RRL}(E) = \frac{1}{2}[1+R(E)]\nu_{\rm L}(E) \\
\nu_{\rm LR}(E) &= \nu_{\rm LLR}(E) + \nu_{\rm RLR}(E) = \frac{1}{2}[1+R(E)]\nu_{\rm R}(E)\ .
\end{aligned} \quad \text{(B16)}$$

In the same way, one can obtain the emissivities of the QPC, however, as they are not needed for this calculation, we do not present them here.

4. Induced charge, bare and screened

As a result of the applied potential and temperature biases, V_α and ΔT_α at the reservoirs $\alpha = $ L,R, charge is injected into the QPC regions. First, the bare charges $Q_{\rm L}^{\rm (b)}$ and $Q_{\rm R}^{\rm (b)}$ on the two QPC regions can be written in terms of the injectivities as

$$\begin{aligned}
Q_{\rm L}^{\rm (b)} &= \mathcal{D}_{\rm LL}V_{\rm L} + \mathcal{D}_{\rm LR}V_{\rm R} + \mathcal{D}^E_{\rm LL}\Delta T_{\rm L} + \mathcal{D}^E_{\rm LR}\Delta T_{\rm R}, \\
Q_{\rm R}^{\rm (b)} &= \mathcal{D}_{\rm RL}V_{\rm L} + \mathcal{D}_{\rm RR}V_{\rm R} + \mathcal{D}^E_{\rm RL}\Delta T_{\rm L} + \mathcal{D}^E_{\rm RR}\Delta T_{\rm R},
\end{aligned} \quad \text{(B17)}$$

Here we have introduced the total, energy integrated charge [34] and entropic [6] injectivities

$$\mathcal{D}_{\alpha\beta} = -e^2\int dE\nu_{\alpha\beta}(E)\frac{df_0}{dE} \quad \text{(B18)}$$

$$\mathcal{D}^E_{\alpha\beta} = -e\int dE\frac{E}{T_0}\nu_{\alpha\beta}(E)\frac{df_0}{dE}. \quad \text{(B19)}$$

Note that the total charge injectivities are given with the units of capacitance.

As a result of the injected charge, the system responds by trying to screen it. In the QPC regions, the electrostatic potentials are shifted $U_{\rm L}$ and $U_{\rm R}$ away from their equilibrium values and screening charges $Q_{\rm L}^{\rm (s)}$ and $Q_{\rm R}^{\rm (s)}$ are induced. Following the same semiclassical approach as for the scattering matrix [36], we can write the screening charges as

$$Q_{\rm L}^{\rm (s)} = -\mathcal{D}_{\rm L}U_{\rm L}, \quad Q_{\rm R}^{\rm (b)} = -\mathcal{D}_{\rm R}U_{\rm R}\ , \quad \text{(B20)}$$

where we introduced the energy integrated, local density of states

$$\mathcal{D}_\alpha = -e^2\int dE\nu_\alpha(E)\frac{df_0}{dE}, \quad \mathcal{D}_{\rm L} = \mathcal{D}_{\rm R} = \frac{\mathcal{D}}{2}. \quad \text{(B21)}$$

Here $\mathcal{D}$ is the total, energy integrated DOS in the system (in the units of capacitance).

The total induced charges in the two regions is then given by the sums of bare and screened charges, $Q_{\rm L} = Q_{\rm L}^{\rm (b)} + Q_{\rm L}^{\rm (s)}$ and $Q_{\rm R} = Q_{\rm R}^{\rm (b)} + Q_{\rm R}^{\rm (s)}$, giving

$$\begin{aligned}
Q_{\rm L} &= \mathcal{D}_{\rm LL}V_{\rm L} + \mathcal{D}_{\rm LR}V_{\rm R} + \mathcal{D}^E_{\rm LL}\Delta T_{\rm L} + \mathcal{D}^E_{\rm LR}\Delta T_{\rm R} - \frac{\mathcal{D}}{2}U_{\rm L}, \\
Q_{\rm R} &= \mathcal{D}_{\rm RL}V_L + \mathcal{D}_{\rm RR}V_{\rm R} + \mathcal{D}^E_{\rm RL}\Delta T_{\rm L} + \mathcal{D}^E_{\rm RR}\Delta T_{\rm R} - \frac{\mathcal{D}}{2}U_{\rm R}.
\end{aligned} \quad \text{(B22)}$$

As a next step, we take into account that the total charges $Q_{\rm L}$ and $Q_{\rm R}$ also couple capacitively to nearby metallic gates and reservoirs, as well as to each other. For the QPC system, the most relevant capacitive couplings are shown in the left panel of Fig. 7. As a result of the capacitive interactions, shown schematically in the right panel of Fig. 7, there will be charges induced on the surfaces of the metallic gates and reservoirs, such that inside a Gauss region [2] the total charge is zero.

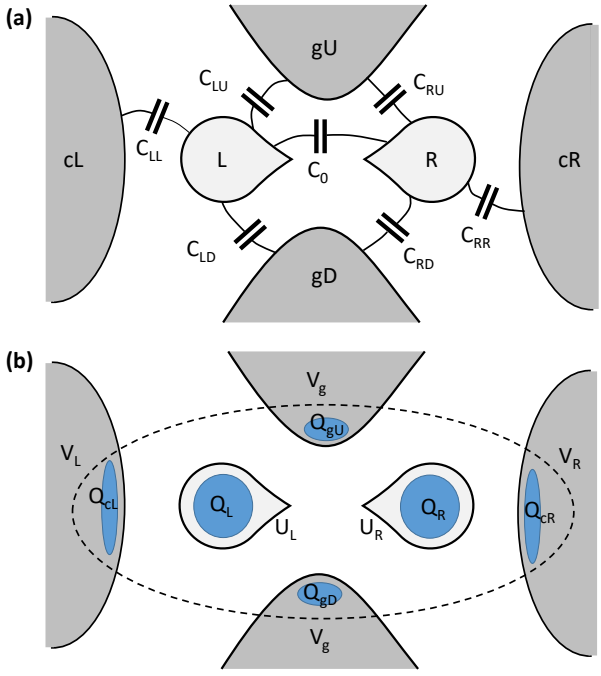

Figure 7. (a) Most relevant geometric capacitances in the system. (b) Induced charges, in QPC and on nearby metallic gates and reservoirs. The Gauss region, inside which the total charge is zero, is shown with dashed lines.

We can thus write the electrostatical relations

$$\begin{aligned} Q_{\rm L} &= C_{\rm LL}(U_{\rm L}-V_{\rm L})+C_{\rm LU}(U_{\rm L}-V_{\rm g})+C_{\rm LD}(U_{\rm L}-V_{\rm g}) \\ &\quad + C_0(U_{\rm L}-U_{\rm R}) \\ Q_{\rm R} &= C_{\rm RR}(U_{\rm R}-V_{\rm R})+C_{\rm RU}(U_{\rm R}-V_{\rm g})+C_{\rm RD}(U_{\rm R}-V_{\rm g}) \\ &\quad + C_0(U_{\rm R}-U_{\rm L}), \end{aligned} \tag{B23}$$

where we have assumed that the same potential $V_{\rm g}$ is applied to both gate electrodes (as is normally the case for a split gate). We can now combine the expressions for the charge in Eqs. (B22) and (B23), giving relations for the induced potentials $U_{\rm L}$ and $U_{\rm R}$ in terms of the applied voltages $V_{\rm L}, V_{\rm R}$, temperatures $\Delta T_{\rm L}, \Delta T_{\rm R}$ and the gate voltage $V_{\rm g}$, in a matrix form as

$$\begin{aligned} \begin{pmatrix} U_{\rm L} \\ U_{\rm R} \end{pmatrix} &= \begin{pmatrix} \xi_{\rm LL} & \xi_{\rm LR} \\ \xi_{\rm RL} & \xi_{\rm RR} \end{pmatrix} \begin{pmatrix} V_{\rm L} \\ V_{\rm R} \end{pmatrix} + \begin{pmatrix} v_{\rm L} \\ v_{\rm R} \end{pmatrix} V_{\rm g} \\ &\quad + \begin{pmatrix} \chi_{\rm LL} & \chi_{\rm LR} \\ \chi_{\rm RL} & \chi_{\rm RR} \end{pmatrix} \begin{pmatrix} \Delta T_{\rm L} \\ \Delta T_{\rm R} \end{pmatrix}. \end{aligned} \tag{B24}$$

The coefficients $\xi_{\alpha\beta}, \chi_{\alpha\beta}$ and v_α are the characteristic potentials we need for the further evaluation. An explicit calculation gives for the voltage ones

$$\begin{aligned} \xi_{\rm LL} &= \frac{1}{Z}[(2C_{\rm R}+2C_{\rm RR}+\mathcal{D})(C_{\rm LL}+\mathcal{D}_{\rm LL}) \\ &\quad + 2C_0(C_{\rm LL}+\mathcal{D}_{\rm LL}+\mathcal{D}_{\rm RL})] \\ \xi_{\rm RL} &= \frac{1}{Z}[(2C_{\rm L}+2C_{\rm LL}+\mathcal{D})\mathcal{D}_{\rm RL} \\ &\quad + 2C_0(C_{\rm LL}+\mathcal{D}_{\rm LL}+\mathcal{D}_{\rm RL})] \\ \xi_{\rm RR} &= \frac{1}{Z}[2C_{\rm L}+2C_{\rm LL}+\mathcal{D})(C_{\rm RR}+D_{\rm RR} \\ &\quad + 2C_0(C_{\rm RR}+\mathcal{D}_{\rm LR}+\mathcal{D}_{\rm RR})] \\ \xi_{\rm LR} &= \frac{1}{Z}[(2C_{\rm R}+2C_{\rm RR}+\mathcal{D})\mathcal{D}_{\rm LR} \\ &\quad + 2C_0(C_{\rm RR}+\mathcal{D}_{\rm LR}+\mathcal{D}_{\rm RR})] \end{aligned} \tag{B25}$$

where we introduced $C_{\rm L}=C_{\rm LD}+C_{\rm LU}, C_{\rm R}=C_{\rm RD}+C_{\rm RU}$ and the denominator

$$\begin{aligned} Z &= 2C_0(C_{\rm L}+C_{\rm LL}+C_{\rm R}+C_{\rm RR}+\mathcal{D}) \\ &\quad + \frac{1}{2}(2C_{\rm L}+2C_{\rm LL}+\mathcal{D})(2C_{\rm R}+2C_{\rm RR}+\mathcal{D}) \end{aligned} \tag{B26}$$

For the temperature ones we get

$$\begin{aligned} \chi_{\rm LL} &= \frac{(2C_{\rm R}+2C_{\rm RR}+\mathcal{D})\mathcal{D}^E_{\rm LL}+2C_0(\mathcal{D}^E_{\rm LL}+\mathcal{D}^E_{\rm RL})}{Z} \\ \chi_{\rm RL} &= \frac{(2C_{\rm L}+2C_{\rm LL}+\mathcal{D})\mathcal{D}^E_{\rm RL}+2C_0(\mathcal{D}^E_{\rm LL}+\mathcal{D}^E_{\rm RL})}{Z} \\ \chi_{\rm RR} &= \frac{(2C_{\rm L}+2C_{\rm LL}+\mathcal{D})\mathcal{D}^E_{\rm RR}+2C_0(\mathcal{D}^E_{\rm LR}+\mathcal{D}^E_{\rm RR})}{Z} \\ \chi_{\rm LR} &= \frac{(2C_{\rm R}+2C_{\rm RR}+\mathcal{D})\mathcal{D}^E_{\rm LR}+2C_0(\mathcal{D}^E_{\rm LR}+\mathcal{D}^E_{\rm RR})}{Z} \end{aligned} \tag{B27}$$

and for the gate potential ones

$$\begin{aligned} v_{\rm L} &= \frac{2C_0(C_{\rm L}+C_{\rm R})+C_{\rm L}(2C_{\rm R}+2C_{\rm RR}+\mathcal{D})}{Z} \\ v_{\rm R} &= \frac{2C_0(C_{\rm L}+C_{\rm R})+C_{\rm R}(2C_{\rm L}+2C_{\rm LL}+\mathcal{D})}{Z}. \end{aligned} \tag{B28}$$

We point out that in the limit considered by Meair and Jacquod [38], our result reduces to theirs.

5. Transport quantities, weak non-linear expansion

The electrical and energy/heat currents both depend on the transmission probability $D(E)$. Away from equilibrium, in the presence of electrical and/or thermal bias, the transmission probability becomes dependent on the applied biases $V_{\rm L}, V_{\rm R}$ and $\Delta T_{\rm L}, \Delta T_{\rm R}$. The equilibrium value of the gate potential is used to regulate the barrier top energy ϵ and the width, determining γ. Throughout the discussion we keep the gate potential constant, at its equilibrium value, i.e. $V_{\rm g}=0$. As discussed above, the applied biases affect the scattering properties by modifying the potentials $U_{\rm L}, U_{\rm R}$, that is, we can write

$$D(E) \equiv D(E, U_{\rm L}[\{V_\alpha, \Delta T_\alpha\}], U_{\rm R}[\{V_\alpha, \Delta T_\alpha\}]), \tag{B29}$$

where $\{V_\alpha, \Delta T_\alpha\} = V_{\rm L}, V_{\rm R}, \Delta T_{\rm L}, \Delta T_{\rm R}$. Within the weakly non-linear approximation we expand $D(E)$ to leading order in the biases, as

$$\begin{aligned} D(E) &\equiv D_0(E) + \frac{\partial D(E)}{\partial U_{\rm L}}\left(\frac{\partial U_{\rm L}}{\partial V_{\rm L}}V_{\rm L}+\frac{\partial U_{\rm L}}{\partial V_{\rm R}}V_{\rm R}\right. \\ &\quad \left. + \frac{\partial U_{\rm L}}{\partial \Delta T_{\rm R}}\Delta T_{\rm R}+\frac{\partial U_{\rm L}}{\partial \Delta T_{\rm L}}\Delta T_{\rm L}\right) + \frac{\partial D(E)}{\partial U_R}\left(\frac{\partial U_R}{\partial V_L}V_L\right. \\ &\quad \left. + \frac{\partial U_{\rm R}}{\partial V_{\rm R}}V_{\rm R}+\frac{\partial U_{\rm R}}{\partial \Delta T_{\rm R}}\Delta T_{\rm R}+\frac{\partial U_{\rm R}}{\partial \Delta T_{\rm L}}\Delta T_{\rm L}\right), \end{aligned} \tag{B30}$$

where $D_0(E)$ is the equilibrium transmission probability in Eq. (1) and all partial derivatives are evaluated at $\{V_\alpha, \Delta T_\alpha\}=0$. Making use of the characteristic potentials we can write, collecting the bias terms,

$$\begin{aligned} D(E) &\equiv D_0(E) + \left(\frac{\partial D(E)}{\partial U_{\rm L}}\xi_{\rm LL}+\frac{\partial D(E)}{\partial U_{\rm R}}\xi_{\rm RL}\right)V_{\rm L} \\ &\quad + \left(\frac{\partial D(E)}{\partial U_{\rm L}}\xi_{\rm RL}+\frac{\partial D(E)}{\partial U_{\rm R}}\xi_{\rm RR}\right)V_{\rm R} \\ &\quad + \left(\frac{\partial D(E)}{\partial U_{\rm L}}\chi_{\rm LL}+\frac{\partial D(E)}{\partial U_{\rm R}}\chi_{\rm RL}\right)\Delta T_{\rm L} \\ &\quad + \left(\frac{\partial D(E)}{\partial U_{\rm L}}\chi_{\rm RL}+\frac{\partial D(E)}{\partial U_{\rm R}}\chi_{\rm RR}\right)\Delta T_{\rm R}. \end{aligned} \tag{B31}$$

Now, it can be shown that gauge invariance guarantees [2, 35] the relation

$$\frac{\partial D(E)}{\partial V_{\rm L}}+\frac{\partial D(E)}{\partial V_{\rm R}}+\frac{\partial D(E)}{\partial V_{\rm g}}+e\frac{\partial D(E)}{\partial E}=0. \tag{B32}$$

Written in terms of the characteristic potentials we have

$$\begin{aligned} &\frac{\partial D(E)}{\partial U_{\rm L}}(\xi_{\rm LL}+\xi_{\rm LR}+v_{\rm L})+\frac{\partial D(E)}{\partial U_{\rm R}}(\xi_{\rm RL}+\xi_{\rm RR}+v_{\rm R}) \\ &= -e\frac{\partial D(E)}{\partial E}. \end{aligned} \tag{B33}$$

Then, using the condition that the sum of the characteristic potential at a given region is unity, gives

$$\xi_{\rm LL}+\xi_{\rm LR}+v_{\rm L}=1,\quad \xi_{\rm RL}+\xi_{\rm RR}+\xi_{\rm R}=1 \tag{B34}$$

and hence

$$\frac{\partial D(E)}{\partial U_{\rm L}}+\frac{\partial D(E)}{\partial U_{\rm R}}=-e\frac{\partial D(E)}{\partial E}. \tag{B35}$$

Following our assumption that the QPC scattering potential is symmetric around $x=0$ we can write

$$\frac{\partial D(E)}{\partial U_{\rm L}}=\frac{\partial D(E)}{\partial U_{\rm R}}=-\frac{e}{2}\frac{\partial D(E)}{\partial E}. \tag{B36}$$

Inserting this into the expression for $D(E)$ we arrive at ($V_{\rm g}=0$),

$$\begin{aligned}D(E)\equiv D_0(E)-\frac{e}{2}\frac{\partial D(E)}{\partial E}(\xi_{\rm L}V_{\rm L}+\xi_{\rm R}V_{\rm R}\\ +\chi_{\rm L}\Delta T_{\rm L}+\chi_{\rm R}\Delta_{\rm R}),\end{aligned} \tag{B37}$$

where we introduced, for shortness, $\xi_{\rm L}=\xi_{\rm LL}+\xi_{\rm RL},\xi_{\rm R}=\xi_{\rm RR}+\xi_{\rm LR},\chi_{\rm L}=\chi_{\rm LL}+\chi_{\rm RL}$ and $\chi_{\rm R}=\chi_{\rm RR}+\chi_{\rm LR}$.

6. Symmetric setup

For the completely symmetric capacitive situation considered in the main text, we have $C_{\rm L}=C_{\rm R}\equiv C_{\rm g}$, $C_{\rm LL}=C_{\rm RR}\equiv C$. As is also clear from the discussion above, we can write the DOS expressions $\mathcal{D}_{\rm LR}=\mathcal{D}_{\rm RL},\mathcal{D}_{\rm RR}=\mathcal{D}_{\rm LL}$ and $\mathcal{D}^E_{\rm LR}=\mathcal{D}^E_{\rm RL},\mathcal{D}^E_{\rm RR}=\mathcal{D}^E_{\rm LL}$. This together allows us to write the relevant characteristic potentials

$$\xi_{\rm L}=\xi_{\rm R}=\frac{2C+\mathcal{D}}{2C+\mathcal{D}+2C_{\rm g}},\quad \chi_{\rm L}=\chi_{\rm R}=\frac{\mathcal{D}^E}{2C+\mathcal{D}+2C_{\rm g}}, \tag{B38}$$

noting that $\mathcal{D}/2=\mathcal{D}_{\rm LL}+\mathcal{D}_{\rm LR}$ and $\mathcal{D}^E/2=\mathcal{D}^E_{\rm LL}+\mathcal{D}^E_{\rm LR}$. We note that, due to the symmetric setup, neither $\xi_{\rm L},\xi_{\rm R}$ nor $\chi_{\rm L},\chi_{\rm R}$ are dependent on C_0. Performing a rescaling $\mathcal{D}^E\to(k_{\rm B}/e)\mathcal{D}^E$ and putting $\xi\equiv\xi_{\rm L}=\xi_{\rm R},\chi\equiv(e/k_{\rm B})\chi_{\rm L}=(e/k_{\rm B})\chi_{\rm R}$, we arrive at Eq. (6) in the main text.

Making use of Eqs. (3) in the main text, we can then directly write down the linear response (in voltage and temperature) modifications of the charge and energy currents due to the SES. For the biasing arrangements discussed in the main text, $V_{\rm L}=0,V_{\rm R}=V,\Delta T_{\rm L}=0,\Delta T_{\rm R}=\Delta T$, we get

$$\begin{aligned}\delta I_{\rm s}&=-\frac{e^2}{2h}\left(\xi V+\frac{k_{\rm B}\chi}{e}\Delta T\right)\\ &\times\sum_{n=-\infty}^{\infty}|S_n|^2\int dE\frac{\partial D_0(E)}{\partial E}\left[f_0(E)-f_0(E_n)\right]\\ \delta I^E_{\rm s}&=-\frac{e}{2h}\left(\xi V+\frac{k_{\rm B}\chi}{e}\Delta T\right)\\ &\times\sum_{n=-\infty}^{\infty}|S_n|^2\int dE\frac{\partial D_0(E)}{\partial E}E\left[f_0(E)-f_0(E_n)\right].\end{aligned} \tag{B39}$$

From these expressions we directly arrive at the expressions for G_s,$L_{\rm s}$, $M_{\rm s}$ and $K_{\rm s}$ in Eq. (10) in the paper.

7. Weak thermoelectric effect

It is particularly interesting to investigate the case with a weak thermoelectric effect, resulting from a weakly energy dependent transmission probability, expanded as

$$\begin{aligned}D_0(E)&=D_0+E\left.\frac{\partial D_0}{\partial E}\right|_{E=E_0}+\frac{E^2}{2}\left.\frac{\partial^2 D_0}{\partial E^2}\right|_{E=E_0}....\\ &\equiv D_0+ED_0'+\frac{E^2}{2}D_0''...\end{aligned} \tag{B40}$$

Keeping only leading order in energy dependence, we have the well known [40] linear response coefficients

$$G=\frac{e^2}{h}D_0,\quad L=-\frac{M}{T_0}=\frac{eT_0}{h}\frac{(\pi k_{\rm B})^2}{3}D_0',\quad K=\mathcal{L}_0T_0G_0 \tag{B41}$$

where $\mathcal{L}_0=(\pi k_{\rm B})^2/(3e^2)$ is the Lorenz number. The direct source currents become (to leading order) independent on the thermoelectric effect, as

$$I^{\rm dir}_{\rm s}=D_0I^{\rm dir}_{\rm s,0},\quad I^{E,{\rm dir}}_{\rm s}=D_0I^{E,{\rm dir}}_{\rm s,0}, \tag{B42}$$

where $I^{\rm dir}_{\rm s,0}$ and $I^{E,{\rm dir}}_{\rm s,0}$ are the bare charge and energy currents of the source. For the source dependent linear response terms, given from Eqs. (10), we get for the conductance

$$\begin{aligned}G_{\rm s}&=-\xi\frac{e^2}{h}\sum_{n=-\infty}^{\infty}|S_n|^2\int dED'\left[f_0(E)-f_0(E_n)\right]\\ &=e\xi D'I^{\rm dir}_{\rm s,0}=\frac{h}{eT_0\mathcal{L}_0}\xi LI^{\rm dir}_{\rm s,0}.\end{aligned} \tag{B43}$$

That is, $G_{\rm s}$ is proportional to the bare source current $I^{\rm dir}_{\rm s,0}$, the thermoelectric coefficient L, and the screening characteristic potential ξ. For the thermoelectric coefficient we get, in the same way

$$L_{\rm s}=\frac{h}{eT_0\mathcal{L}_0}\chi LI^{\rm dir}_{\rm s,0}, \tag{B44}$$

proportional to $G_{\rm s}$. For the energy current terms we have

$$\begin{aligned}M_{\rm s}&=-u_{\rm R}\frac{e}{2h}\sum_{n=-\infty}^{\infty}|S_n|^2\int dED'E\left[f_0(E)-f_0(E_n)\right]\\ &=\frac{e}{2}\chi D'I^{E,{\rm dir}}_{\rm s,0}=\frac{h}{2eT_0\mathcal{L}_0}\chi LI^{E,{\rm dir}}_{\rm s,0}.\end{aligned} \tag{B45}$$

and, in the same way,

$$K_{\rm s}=\frac{h}{2eT_0\mathcal{L}_0}\chi LI^{\rm dir}_{\rm s,E}. \tag{B46}$$

The expressions for $G_{\rm s}$ and $M_{\rm s}$ are the ones given in Eq. (13) in the main text.

8. Key integrals

Two integral expressions are of key importance for the numerical evaluation of ξ and χ. From Eqs. (B11) and (B12) we have

$$\mathcal{D} = \frac{e^2}{4\pi k_{\rm B}T_0\gamma}\int_{\epsilon-E_\lambda}^{\epsilon} dE \frac{\operatorname{arcosh}\left(\sqrt{E_\lambda/(\epsilon-E)}\right)}{\cosh(E/[2k_{\rm B}T_0])} + \frac{e^2}{4\pi k_{\rm B}T_0\gamma}\int_{\epsilon}^{\infty} dE \frac{\operatorname{arsinh}\left(\sqrt{E_\lambda/(E-\epsilon)}\right)}{\cosh(E/[2k_{\rm B}T_0])}. \quad \text{(B47)}$$

Changing variables as $x = (\epsilon - E)/E_\lambda$ and $y = (E - \epsilon)/E_\lambda$, we get

$$\mathcal{D} = \frac{e^2E_\lambda}{4\pi\gamma k_{\rm B}T_0}\left[\int_0^1 dx\ \operatorname{arcosh}\left(\sqrt{\frac{1}{x}}\right)\frac{1}{\cosh([\epsilon_0 - x\epsilon_\lambda]/2)} + \int_0^\infty dy\ \operatorname{arsinh}\left(\sqrt{\frac{1}{y}}\right)\frac{1}{\cosh([\epsilon_0 + y\epsilon_\lambda]/2)}\right], \quad \text{(B48)}$$

where we introduced the dimensionless energies $\epsilon_\lambda = E_\lambda/[k_{\rm B}T_0]$ and $\epsilon_0 = \epsilon/[k_{\rm B}T_0]$. To have a more shorthand notation we first write

$$\mathcal{D} = 2\mathcal{D}_0\left(\mathcal{F}_0 + \mathcal{G}_0\right), \quad \mathcal{D}_0 = \frac{e^2E_\lambda}{8\pi\gamma k_{\rm B}T_0}, \quad \text{(B49)}$$

where the dimensionless integrals are

$$\mathcal{F}_n = \int_0^1 dx\ x^n \operatorname{arcosh}\left(\sqrt{\frac{1}{x}}\right)\frac{1}{\cosh([\epsilon_0 - x\epsilon_\lambda]/2)}$$
$$\mathcal{G}_n = \int_0^\infty dy\ y^n \operatorname{arsinh}\left(\sqrt{\frac{1}{y}}\right)\frac{1}{\cosh([\epsilon_0 + y\epsilon_\lambda]/2)}. \quad \text{(B50)}$$

In this notation, convenient for the numerics, we can write the characteristic potential

$$\xi = \frac{1 + \frac{\mathcal{D}}{2C}}{1 + \frac{\mathcal{D}}{2C} + \frac{C_g}{C}} = \frac{1 + c_d(\mathcal{F}_0 + \mathcal{G}_0)}{1 + c_g + c_d(\mathcal{F}_0 + \mathcal{G}_0)}, \quad \text{(B51)}$$

introducing yet another shorthand notation with dimensionless quantities $c_d = \mathcal{D}_0/C, c_g = C_g/C$. This form shows clearly the different, independent dimensionless parameters that controls ξ, namely $\epsilon_\lambda, \epsilon_0, c_g, c_d$.

In the same way we have

$$\mathcal{D}^E = \frac{e^2}{4\pi\gamma k_{\rm B}^2T_0}\int_{\epsilon-E_\lambda}^{\epsilon} dE \frac{E}{T_0}\frac{\operatorname{arcosh}\left(\sqrt{E_\lambda/(\epsilon-E)}\right)}{\cosh(E/[2k_{\rm B}T_0])} + \frac{e^2}{4\pi\gamma k_{\rm B}^2T_0}\int_{\epsilon}^{\infty} dE \frac{E}{T_0}\frac{\operatorname{arsinh}\left(\sqrt{E_\lambda/(E-\epsilon)}\right)}{\cosh(E/[2k_{\rm B}T_0])}. \quad \text{(B52)}$$

Making the same variable substitutions as for $\mathcal{D}$ we have

$$\mathcal{D}^E = 2\mathcal{D}_0\left[\epsilon_0\left(\mathcal{F}_0 + \mathcal{G}_0\right) + \epsilon_\lambda\left(-\mathcal{F}_1 + \mathcal{G}_1\right)\right] \quad \text{(B53)}$$

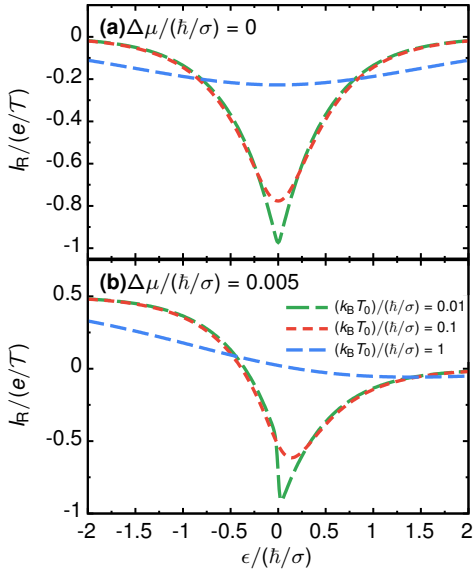

Figure 8. Charge current as a function of $\epsilon/(\hbar/\sigma)$ for different values $k_{\rm B}T_0/(\hbar/\sigma)$ and $\Delta T = 0$, when (a) $\Delta\mu/(\hbar/\sigma) = 0$ and (b) $\Delta\mu/(\hbar/\sigma) = 0.005$.

We can thus write the relevant, dimensionless characteristic potential function

$$\chi = \frac{\mathcal{D}^E}{2C + \mathcal{D} + 2C_g} = \frac{c_d\left[\epsilon_0\left(\mathcal{F}_0 + \mathcal{G}_0\right) + \epsilon_\lambda\left(-\mathcal{F}_1 + \mathcal{G}_1\right)\right]}{1 + c_g + c_d(\mathcal{F}_0 + \mathcal{G}_0)}. \quad \text{(B54)}$$

We note that since the integrals $\mathcal{F}_n$ and $\mathcal{G}_n$ are functions of ϵ_0 and ϵ_λ, the same four parameters $\epsilon_0, \epsilon_\lambda, c_d$ and c_g determine both ξ and $e\chi/k_{\rm B}$.

Appendix C: Linear response charge and heat currents – sharp barrier

In this appendix we show analytical results for all contributions to Eq. (7) for the case where the QPC transmission is approximated by a sharp step function. Note that in this case, it is useful to neglect all *quantum screening* effects and to assume symmetric, geometrical capacitances leading to $\xi = \frac{1}{2}$. For the standard, stationary response coefficients, we find

$$G = \frac{e^2}{h}f_0(\epsilon), \quad \text{(C1)}$$

$$L = -\frac{M}{T_0} = \frac{e}{h}\frac{1}{T_0}\left[\epsilon(f_0(\epsilon) - 1) - k_{\rm B}T_0\ \ln\{f_0(\epsilon)\}\right], \quad \text{(C2)}$$

$$K = -\frac{1}{h}\frac{1}{T_0}\left[\epsilon^2(f_0(\epsilon) - 1) - 2k_{\rm B}T_0\,\epsilon\ln\{f_0(\epsilon)\} + 2(k_{\rm B}T_0)^2{\rm Li}_2\left\{-e^{\frac{\epsilon}{k_{\rm B}T_0}}\right\} + \frac{(\pi k_{\rm B}T_0)^2}{3}\right]. \quad \text{(C3)}$$

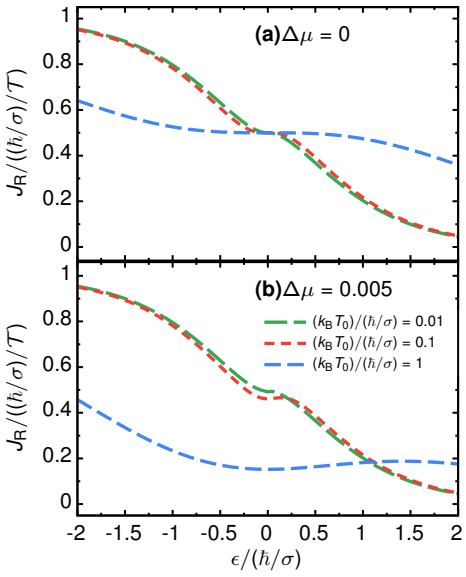

Figure 9. Heat current as a function of $\epsilon/(\hbar/\sigma)$ for different values $k_{\rm B}T_0/(\hbar/\sigma)$ and $\Delta T = 0$, when (a) $\Delta\mu/(\hbar/\sigma) = 0$ and (b) $\Delta\mu/(\hbar/\sigma) = 0.005$.

For the currents injected from the source, which are independent of the applied biases, we find

$$I_{\rm s}^{\rm dir} = \frac{e}{h}\sum_{n>0}|S_n|^2\left\{k_{\rm B}T_0\ln\left\{\frac{f_0(\epsilon+n\hbar\Omega)}{f_0(\epsilon)}\right\}\right\}, \tag{C4}$$

$$\begin{aligned} I_{\rm s}^{E,\rm dir} = &-\frac{1}{h}\sum_{n=-\infty}^{\infty}|S_n|^2\Big\{-(n\hbar\Omega)^2 \\ &+ k_{\rm B}T_0\,\epsilon\left[\ln\left\{\frac{f_0(\epsilon+n\hbar\Omega)}{f_0(\epsilon)}\right\}+\ln\left\{\frac{f_0(\epsilon-n\hbar\Omega)}{f_0(\epsilon)}\right\}\right] \\ &+ (k_{\rm B}T_0)^2\left[{\rm Li}_2\left\{-e^{\frac{\epsilon}{k_{\rm B}T_0}}\right\}-{\rm Li}_2\left\{-e^{\frac{\epsilon+n\hbar\Omega}{k_{\rm B}T_0}}\right\}\right] \\ &+ (k_{\rm B}T_0)^2\left[{\rm Li}_2\left\{-e^{\frac{\epsilon}{k_{\rm B}T_0}}\right\}-{\rm Li}_2\left\{-e^{\frac{\epsilon-n\hbar\Omega}{k_{\rm B}T_0}}\right\}\right]\Big\}. \end{aligned} \tag{C5}$$

Finally, we present results for the modification of the linear response coefficients due to the discussed interplay between screening effects and time-dependent driving

$$G_{\rm s} = \frac{e^2}{2h}\sum_{n>0}|S_n|^2\left[-2f_0(\epsilon)+f_0(\epsilon+n\hbar\Omega)+f_0(\epsilon-n\hbar\Omega)\right], \tag{C6}$$

$$\begin{aligned} M_{\rm s} = &-\frac{e}{2h}\sum_{n>0}|S_n|^2 \\ &\Big[\epsilon\left[-2f_0(\epsilon)+f_0(\epsilon+n\hbar\Omega)+f_0(\epsilon-n\hbar\Omega)\right] \\ &+ 2k_{\rm B}T_0\ln\left\{\frac{f_0(\epsilon)}{f_0(\epsilon+n\hbar\Omega)}\right\}+2k_{\rm B}T_0\ln\left\{\frac{f_0(\epsilon)}{f_0(\epsilon-n\hbar\Omega)}\right\}\Big]. \end{aligned} \tag{C7}$$

The missing coefficients $L_{\rm s}$ and $K_{\rm s}$ are zero in the absence of quantum screening and are otherwise straightforwardly obtained from Eq. (12).

In the following we show results, in Fig. 8, for the obtained currents for the case where no temperature bias, but only a voltage bias is applied. This means in particular

$$I_{\rm R} = (G+G_{\rm s})V + I_{\rm s}^{\rm dir} \tag{C8}$$

$$J_{\rm R} = (M+M_{\rm s})V + I_{\rm s}^{E,\rm dir}. \tag{C9}$$

In Fig. 8 panel (a), we show the case of vanishing potential bias; the charge current is then given by the direct current from the source alone. When applying an electrochemical potential, Fig. 8 (b), when $\epsilon \ll 0$, meaning that the energy filtering by the transmission function is negligible, the conductance G is the main contribution to the charge current. The charge current of the source is zero because of the (approximate) electron-hole symmetry. However at small, but positive step energies, the direct current from the source is maximal. It therefore at low temperatures dominates the total charge current. At high temperatures, $k_{\rm B}T_0 > \hbar/\sigma$, the effect of the source is negligible, and again, the conductance G, becomes the key contribution to the charge current.

Similarly, the dominating influence of the thermoelectric coefficient M and the direct source energy current can be observed in the heat current up to linear response, as shown in Fig. 9.

[1] G. Benenti, G. Casati, K. Saito, and R. S. Whitney, "Fundamental aspects of steady-state conversion of heat to work at the nanoscale," Phys. Rep. **694**, 1–124 (2017).

[2] T. Christen and M. Büttiker, "Gauge-invariant nonlinear electric transport in mesoscopic conductors," EPL **35**, 523–528 (1996).

[3] M. Büttiker and D. Sánchez, "Interaction-induced magnetic field asymmetry of nonlinear mesoscopic electrical transport," Int. J. Quantum Chem. **105**, 906–913 (2005).

[4] M. Büttiker and T. Christen, "Admittance and Nonlinear Transport in Quantum Wires, Point Contacts, and Resonant Tunneling Barriers," SpringerLink , 259–289 (1997).

[5] D. Sánchez and M. Büttiker, "Magnetic-Field Asymmetry of Nonlinear Mesoscopic Transport," Phys. Rev. Lett. **93**, 106802 (2004).

[6] D. Sánchez and R. López, "Scattering Theory of Nonlinear Thermoelectric Transport," Phys. Rev. Lett. **110**, 026804 (2013).

[7] J. Gabelli, G. Fève, J.-M. Berroir, B. Plaçais, A. Cavanna, B. Etienne, Y. Jin, and D. C. Glattli, "Violation of Kirchhoff's Laws for a Coherent RC Circuit," Science **313**, 499–502 (2006).

[8] J. P. Pekola, O.-P. Saira, V. F. Maisi, A. Kemppinen,

M. Möttönen, Y. A. Pashkin, and D. V. Averin, "Single-electron current sources: Toward a refined definition of the ampere," Rev. Mod. Phys. **85**, 1421–1472 (2013).
[9] E. Bocquillon, V. Freulon, F. D. Parmentier, J.-M. Berroir, B. Plaçais, C. Wahl, J. Rech, T. Jonckheere, T. Martin, C. Grenier, D. Ferraro, P. Degiovanni, and G. Fève, "Electron quantum optics in ballistic chiral conductors," Ann. Phys. **526**, 1–30 (2014).
[10] C. Bäuerle, D. C. Glattli, T. Meunier, F. Portier, P. Roche, P. Roulleau, S. Takada, and X. Waintal, "Coherent control of single electrons: a review of current progress," Rep. Prog. Phys. **81**, 056503 (2018).
[11] M. Vanević, Y. V. Nazarov, and W. Belzig, "Elementary Events of Electron Transfer in a Voltage-Driven Quantum Point Contact," Phys. Rev. Lett. **99**, 076601 (2007).
[12] M. Vanević, Y. V. Nazarov, and W. Belzig, "Elementary charge-transfer processes in mesoscopic conductors," Phys. Rev. B **78**, 245308 (2008).
[13] M. Vanević and W. Belzig, "Control of electron-hole pair generation by biharmonic voltage drive of a quantum point contact," Phys. Rev. B **86**, 241306 (2012).
[14] J. Gabelli and B. Reulet, "Shaping a time-dependent excitation to minimize the shot noise in a tunnel junction," Phys. Rev. B **87**, 075403 (2013).
[15] J. Dubois, T. Jullien, F. Portier, P. Roche, A. Cavanna, Y. Jin, W. Wegscheider, P. Roulleau, and D. C. Glattli, "Minimal-excitation states for electron quantum optics using levitons," Nature **502**, 659–663 (2013).
[16] N. Dashti, M. Misiorny, P. Samuelsson, and J. Splettstoesser, "Probing charge- and heat-current noise by frequency-dependent fluctuations in temperature and potential," Phys. Rev. Appl. **10**, 024007 (2018).
[17] F. Battista, M. Moskalets, M. Albert, and P. Samuelsson, "Quantum Heat Fluctuations of Single-Particle Sources," Phys. Rev. Lett. **110**, 126602 (2013).
[18] M. Moskalets, "Floquet Scattering Matrix Theory of Heat Fluctuations in Dynamical Quantum Conductors," Phys. Rev. Lett. **112**, 206801 (2014).
[19] M. Moskalets, "Erratum: Floquet Scattering Matrix Theory of Heat Fluctuations in Dynamical Quantum Conductors [Phys. Rev. Lett. 112, 206801 (2014)]," Phys. Rev. Lett. **113**, 069902 (2014).
[20] F. Battista, F. Haupt, and J. Splettstoesser, "Energy and power fluctuations in ac-driven coherent conductors," Phys. Rev. B **90**, 085418 (2014).
[21] F. Battista, F. Haupt, and J. Splettstoesser, "Correlations between charge and energy current in ac-driven coherent conductors," J. Phys. Conf. Ser. **568**, 052008 (2014).
[22] L. Vannucci, F. Ronetti, J. Rech, D. Ferraro, T. Jonckheere, T. Martin, and M. Sassetti, "Minimal excitation states for heat transport in driven quantum Hall systems," Phys. Rev. B **95**, 245415 (2017).
[23] J. D. Fletcher, P. See, H. Howe, M. Pepper, S. P. Giblin, J. P. Griffiths, G. A. C. Jones, I. Farrer, D. A. Ritchie, T. J. B. M. Janssen, and M. Kataoka, "Clock-Controlled Emission of Single-Electron Wave Packets in a Solid-State Circuit," Phys. Rev. Lett. **111**, 216807 (2013).
[24] N. Ubbelohde, F. Hohls, V. Kashcheyevs, T. Wagner, L. Fricke, B. Kästner, K. Pierz, H. W. Schumacher, and R. J. Haug, "Partitioning of on-demand electron pairs," Nat. Nanotechnol. **10**, 46–49 (2015).
[25] T. Jullien, P. Roulleau, B. Roche, A. Cavanna, Y. Jin, and D. C. Glattli, "Quantum tomography of an electron," Nature **514**, 603–607 (2014).
[26] A. Marguerite, B. Roussel, R. Bisognin, C. Cabart, M. Kumar, J.-M. Berroir, E. Bocquillon, B. Plaçais, A. Cavanna, U. Gennser, Y. Jin, P. Degiovanni, and G. Fève, "Extracting single electron wavefunctions from a quantum electrical current," arXiv (2017), 1710.11181.
[27] M. Büttiker, "Quantized transmission of a saddle-point constriction," Phys. Rev. B **41**, 7906–7909 (1990).
[28] H. van Houten, L. W. Molenkamp, C. W. J. Beenakker, and C. T. Foxon, "Thermo-electric properties of quantum point contacts," Semicond. Sci. Technol. **7**, B215–B221 (1992).
[29] R. S. Whitney, "Most Efficient Quantum Thermoelectric at Finite Power Output," Phys. Rev. Lett. **112**, 130601 (2014).
[30] R. S. Whitney, "Finding the quantum thermoelectric with maximal efficiency and minimal entropy production at given power output," Phys. Rev. B **91**, 115425 (2015).
[31] M. Büttiker, H. Thomas, and A. Prêtre, "Mesoscopic capacitors," Phys. Lett. A **180**, 364–369 (1993).
[32] A. Prêtre, H. Thomas, and M. Büttiker, "Dynamic admittance of mesoscopic conductors: Discrete-potential model," Phys. Rev. B **54**, 8130–8143 (1996).
[33] G. Fève, A. Mahé, J.-M. Berroir, T. Kontos, B. Plaçais, D. C. Glattli, A. Cavanna, B. Etienne, and Y. Jin, "An On-Demand Coherent Single-Electron Source," Science **316**, 1169–1172 (2007).
[34] M. Büttiker, A. Prêtre, and H. Thomas, "Dynamic conductance and the scattering matrix of small conductors," Phys. Rev. Lett. **70**, 4114–4117 (1993).
[35] M. Buttiker, "Capacitance, admittance, and rectification properties of small conductors," J. Phys.: Condens. Matter **5**, 9361–9378 (1993).
[36] T. Christen and M. Büttiker, "Low Frequency Admittance of a Quantum Point Contact," Phys. Rev. Lett. **77**, 143–146 (1996).
[37] M. H. Pedersen, S. A. van Langen, and M. Büttiker, "Charge fluctuations in quantum point contacts and chaotic cavities in the presence of transport," Phys. Rev. B **57**, 1838–1846 (1998).
[38] J. Meair and P. Jacquod, "Scattering theory of nonlinear thermoelectricity in quantum coherent conductors," J. Phys.: Condens. Matter **25**, 082201 (2013).
[39] M. Büttiker, "Four-Terminal Phase-Coherent Conductance," Phys. Rev. Lett. **57**, 1761–1764 (1986).
[40] P. N. Butcher, "Thermal and electrical transport formalism for electronic microstructures with many terminals," J. Phys.: Condens. Matter **2**, 4869–4878 (1990).
[41] Ya. M. Blanter and M. Büttiker, "Shot noise in mesoscopic conductors," Phys. Rep. **336**, 1–166 (2000).
[42] M. V. Moskalets, *Scattering Matrix Approach to Non-Stationary Quantum Transport* (Imperial College Press, London, 2011).
[43] J. Dubois, T. Jullien, C. Grenier, P. Degiovanni, P. Roulleau, and D. C. Glattli, "Integer and fractional charge Lorentzian voltage pulses analyzed in the framework of photon-assisted shot noise," Phys. Rev. B **88**, 085301 (2013).
[44] B. Kaestner, V. Kashcheyevs, S. Amakawa, M. D. Blumenthal, L. Li, T. J. B. M. Janssen, G. Hein, K. Pierz, T. Weimann, U. Siegner, and H. W. Schumacher, "Single-parameter nonadiabatic quantized charge pumping," Phys. Rev. B **77**, 153301 (2008).
[45] S. P. Giblin, S. J. Wright, J. D. Fletcher, M. Kataoka,

M. Pepper, T. J. B. M. Janssen, D. A. Ritchie, C. A. Nicoll, D. Anderson, and G. A. C. Jones, "An accurate high-speed single-electron quantum dot pump," New J. Phys. **12**, 073013 (2010).

[46] R. P. G. McNeil, M. Kataoka, C. J. B. Ford, C. H. W. Barnes, D. Anderson, G. A. C. Jones, I. Farrer, and D. A. Ritchie, "On-demand single-electron transfer between distant quantum dots," nature **477**, 439–442 (2011).

[47] S. Hermelin, S. Takada, M. Yamamoto, S. Tarucha, A. D. Wieck, L. Saminadayar, C. Bäuerle, and T. Meunier, "Electrons surfing on a sound wave as a platform for quantum optics with flying electrons," nature **477**, 435–438 (2011).

[48] J. P. Pekola, J. J. Vartiainen, M. Möttönen, O.-P. Saira, M. Meschke, and D. V. Averin, "Hybrid single-electron transistor as a source of quantized electric current," Nat. Phys. **4**, 120–124 (2007).

[49] D. M. T. van Zanten, D. M. Basko, I. M. Khaymovich, J. P. Pekola, H. Courtois, and C. B. Winkelmann, "Single Quantum Level Electron Turnstile," Phys. Rev. Lett. **116**, 166801 (2016).

[50] H. Pothier, P. Lafarge, C. Urbina, D. Esteve, and M. H. Devoret, "Single-Electron Pump Based on Charging Effects," EPL **17**, 249–254 (1992).

[51] S. J. Chorley, J. Frake, C. G. Smith, G. A. C. Jones, and M. R. Buitelaar, "Quantized charge pumping through a carbon nanotube double quantum dot," Appl. Phys. Lett. **100**, 143104 (2012).

[52] B. Roche, R.-P. Riwar, B. Voisin, E. Dupont-Ferrier, R. Wacquez, M. Vinet, M. Sanquer, J. Splettstoesser, and X. Jehl, "A two-atom electron pump," Nat. Commun. **4**, 1581 (2013).

[53] M. R. Connolly, K. L. Chiu, S. P. Giblin, M. Kataoka, J. D. Fletcher, C. Chua, J. P. Griffiths, G. A. C. Jones, V. I. Fal'ko, C. G. Smith, and T. J. B. M. Janssen, "Gigahertz quantized charge pumping in graphene quantum dots," Nat. Nanotechnol. **8**, 417–420 (2013).

[54] E. Bocquillon, F. D. Parmentier, C. Grenier, J.-M. Berroir, P. Degiovanni, D. C. Glattli, B. Plaçais, A. Cavanna, Y. Jin, and G. Fève, "Electron Quantum Optics: Partitioning Electrons One by One," Phys. Rev. Lett. **108**, 196803 (2012).

[55] E. Bocquillon, V. Freulon, J.-M. Berroir, P. Degiovanni, B. Plaçais, A. Cavanna, Y. Jin, and G. Fève, "Coherence and Indistinguishability of Single Electrons Emitted by Independent Sources," Science **339**, 1054–1057 (2013).

[56] E. Bocquillon, V. Freulon, J.-M. Berroir, P. Degiovanni, B. Plaçais, A. Cavanna, Y. Jin, and G. Fève, "Separation of neutral and charge modes in one-dimensional chiral edge channels," Nat. Commun. **4**, 1839 (2013).

[57] N. Dashti, M. Misiorny, S. Kheradsoud, P. Samuelsson, and J. Splettstoesser, "Minimal excitation single-particle emitters: Comparison of charge-transport and energy-transport properties," Phys. Rev. B **100**, 035405 (2019).

[58] H. A. Fertig and B. I. Halperin, "Transmission coefficient of an electron through a saddle-point potential in a magnetic field," Phys. Rev. B **36**, 7969–7976 (1987).

[59] J. N. L. Connor, "On the analytical description of resonance tunnelling reactions," Mol. Phys. **15**, 37–46 (1968).

[60] E. P. Wigner, "Lower Limit for the Energy Derivative of the Scattering Phase Shift," Phys. Rev. **98**, 145–147 (1955).

[61] F. T. Smith, "Lifetime Matrix in Collision Theory," Phys. Rev. **118**, 349–356 (1960).